Research on Hybrid Control Methods for the Path Tracking of Driverless Vehicles

Jingyuan Li, Jianguo Xi, Chengwei Xie, and Jianping Gao

Abstract—**This paper presents a hybrid control strategy that utilizes fuzzy control theory to tackle the issue of suboptimal path tracking performance in autonomous vehicles operating at different speeds. The proposed method integrates an enhanced pure pursuit control approach, with a model predictive control strategy rooted in vehicle dynamics. The method selects different control algorithms depending on the vehicle's speed range, optimizing path tracking performance across different operational conditions. Simulations conducted using the Carsim/Simulink platform demonstrate that, under double-shifted line condition, the peak lateral error is diminished by 18.5%, and the maximum front wheel angle is diminished by 12.3%. In lane-changing curve condition, the peak lateral error is diminished by 17.8%, and the highest front wheel angle is decreased by 17.3%. Under continuous lane-changing curve condition, the peak lateral error decreases by 18.4%, and the peak front wheel angle is reduced by 20%. The experimental findings validate that the proposed hybrid control approach considerably enhances both path tracking precision and vehicle stability under various driving conditions.**

Index Terms—**driverless vehicles, hybrid control, model predictive control, path tracking, pure pursuit control**

I. Introduction

In recent years, the ongoing progress in automotive intelligence has been remarkable, autonomous driving technology has emerged as a globally recognized avenue for future development and a key area of academic research [1], [2]. Path tracking control is fundamental to achieving autonomous driving [3], as it uses the desired target path ahead of the vehicle and the vehicle's state parameters to calculate the necessary steering angle. This allows driverless vehicles to follow the intended path accurately [4].

Currently, the most common methods for path tracking include learning-based control methods [5], Pure Pursuit (PP) control [6], model predictive control (MPC) [7], fuzzy control proportional integral derivative (PID) control [8], sliding mode control [9]. Luo et al. proposed an algorithm, with experimental comparisons demonstrating its effectiveness [10]. Peng et al. designed a computer-controlled steering system [11]. Nahlia et al. modified the Floyd-Warshall algorithm to plan the optimal path of a transportation network, with various parameters represented as a multigraph, using the interval-valued in algorithm tuitionistic fuzzy number method [12]. Zuo et al. introduced an arc prediction method that estimates model deviation [13]. Ma et al. employed a nonlinear predictive control model for Unmanned Ground Vehicle (UGV) steering and speed control [14]. Meanwhile, Bao et al. proposed a genetic algorithm (GA). Simulation experiments demonstrated that the proposed algorithm performs robustly, finding feasible paths within a relatively short time [15].

Nur et al. introduced an innovative method for kinematic modeling for a robotic two-wheeled vehicle [16]. Su et al. proposed a transversely robust iterative learning control method for uncrewed robotic vehicles [17]. Chen et al. combined GA with Iterated Ant Colony Optimization (IACO) to formulate a hybrid approach for quick path determination. They modified the crossover operator to reduce the risk of failure, and simulation results validated the robot's ability to travel safely between points [18]. Han et al. proposed a second-order control system model for a PID controller based on a neural network, designed for transverse path tracking [19]. Hu et al. devised an optimization-based synthetic nonlinear feedback control method to reduce steady-state error in trajectory tracking control [20]. Hong et al. explored a model predictive control method capable of effectively predicting and controlling imminent vehicle swaying through rolling optimization control [21]. Kay et al. designed a linear model predictive controller integrating feedforward and robust control strategies [22]. Recently, deep learning approaches for tracking and controlling autonomous vehicles have attracted considerable attention. Yao et al. introduced a method to ensure the vehicle stays on its pre-planned path [23].

Wang et al. developed a simulated car model that exhibits steering delay characteristics. They implemented MPC path-tracking model in tangential-normal coordinate system, demonstrating effective tracking performance [24]. Zhang et al. developed a longitudinal regulate system, following their proposed method for lateral vehicle control [25]. Chen et al. developed a Linear Quadratic Regulator (LQR) controller to reduce tracking errors [26]. Zhang et al. introduced a linear sliding mode control approach for trajectory tracking, addressing non-matching uncertainties [27]. Liu et al.

Manuscript received August 6, 2024; revised January 2, 2025.

This work was supported in part by the Major Science and Technology Programs of Henan Province, China, under grant number 241100240300.

Jingyuan Li is a postgraduate student at the School of Vehicle and Transportation Engineering, Henan University of Science and Technology, Luoyang 471000, China (email: lzyjcl@163.com).

Jianguo Xi is a senior laboratory technician at the School of Vehicle and Transportation Engineering, Henan University of Science and Technology, Luoyang 471000, China (email: xijianguo@sohu.com).

Chengwei Xie is a doctorate student at the School of Vehicle and Transportation Engineering, Henan University of Science and Technology, Luoyang 471000, China (email: maruyuet@163.com).

Jianping Gao is a professor at the School of Vehicle and Transportation Engineering, Henan University of Science and Technology, Luoyang 471000, China (Corresponding author, email: jyhywan@aliyun.com).

introduced a fuzzy control algorithm for Automated Guided Vehicle (AGV) trajectory tracking, enhancing the tracking performance through the PP control algorithm [28]. Wang et al. formulated an equation relating lateral error to the desired yaw angle, and subsequently constructed a self-immune vehicle lateral control model [29]. Tan Wei et al. introduced a trajectory tracking control approach grounded in robust predictive control, with the goal of enhancing both path tracking accuracy and system robustness [30].

The driving conditions and environments encountered by autonomous vehicles are inherently complex, variable, and fraught with uncertainty. A single control algorithm often struggles to adapt to these diverse conditions, making optimal path tracking difficult to achieve. This study introduces a hybrid control method that integrates various control strategies to achieve precise and reliable path tracking. This approach is particularly effective in handling varying vehicle speeds, road types, and environmental factors, improving performance across a wider range of driving scenarios.

The proposed hybrid control method combines an improved feedback-based pure pursuit control approach with model-based predictive path tracking. A PP method be first proposed founded on the kinematic model. To enhance performance under varying conditions, an improved feedback-based pure pursuit control method is subsequently implemented. Additionally, a path-tracking regulation system is initially suggested built on a kinematic model. Given the varying performance of different methods under different vehicle conditions, a hybrid control approach grounded in fuzzy control theory is introduced. This approach categorizes the vehicle's longitudinal speed into three intervals, with corresponding switching rules defined. Each speed interval is associated with its respective control method, thereby improving path tracking accuracy.

The research and results of this work consist of five parts: The part 2 formulates the kinematic model and a three degree of freedom dynamic model. Part 3 delineates an enhanced feedback-based pure pursuit control approach, alongside the proposal of MPC based controller for path tracking. A collaborative simulation with Carsim and Simulink is subsequently performed to validate and contrast the efficacy of both methodologies. Section 4 presents a hybrid control methodology grounded in fuzzy control theory, utilizing the Simulink platform to construct the simulation model for the switching controller. Section 5 assesses the efficacy of the proposed technique under diverse road circumstances with Carsim/Simulink. Ultimately, part 6 encapsulates the principal conclusions of the work, the overall research process and results are shown below.

II. Construction of the Driverless Vehicle Model

A. Vehicle kinematics modeling

The kinematic-based controller demonstrates superior performance under low-speed conditions, enhancing both accuracy and stability in path tracking. By effectively utilizing the vehicle's kinematic characteristics, it ensures precise and reliable control at lower speeds.

As shown in Fig. 1, the coordinates of the vehicle's center of mass are denoted as（Xc,Yc）, where $(x_f, y_f),(x_r, y_r)$ represent the front and rear axle centers, respectively. v_r denotes the speed of the rear axle center, α is the angle between the vehicle's direction of travel and the X-axis., L is the vehicle's wheelbase, and δ is the steering angle of the front wheels.

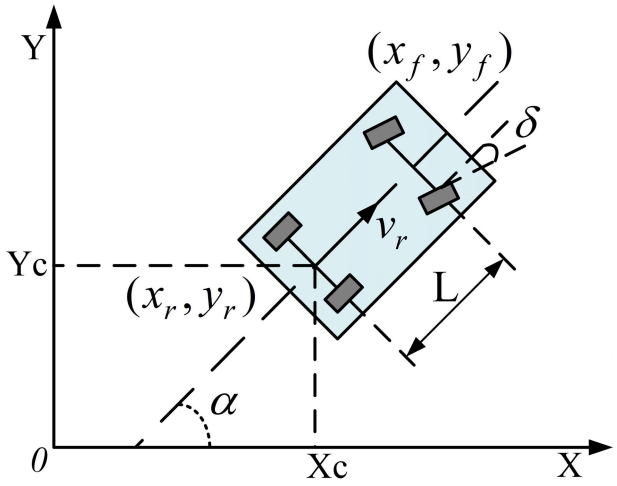

Fig. 1 Kinematics model of vehicle

At the rear axle (Xr,Yr) :

$$v_r = \dot{X}_r \cos\alpha + \dot{Y}_r \sin\alpha \tag{1}$$

$$\begin{cases} \dot{X}_f sin(\alpha+\delta) = \dot{Y}_f cos(\alpha+\delta) \\ \dot{X}_r sin\alpha = \dot{Y}_r cos\alpha \end{cases} \tag{2}$$

The transverse pendulum's angular velocity is:

$$\omega = \frac{v_r \tan\delta}{L} \tag{3}$$

The vehicle's kinematic model can be obtained as follows:

$$\begin{bmatrix} X_r \\ Y_r \\ \alpha \end{bmatrix} = \begin{bmatrix} \cos\alpha \\ \sin\alpha \\ tan\delta / L \end{bmatrix} v_r \tag{4}$$

B. Vehicle dynamics modeling

As illustrated in Fig. 2, a three-degree-of-freedom vehicle dynamics model is developed. The assumptions are as follows:

1) The driverless vehicle is assumed to be traveling on a flat road surface.

2) The tires are assumed to operate within their linear range, without accounting for the interaction between the lateral and longitudinal directions.

3) Air resistance is neglected in all directions.

4) It is assumed that the rear wheels have a zero-steering angle, and the vehicle relies solely on the front wheels for steering.

5) The vehicle and its suspension system are idealized as rigid bodies, neglecting any effects of suspension dynamics.

6) The vehicle is represented as a simplified system with two axles, neglecting the influence of the wheels spacing on the turning radius.

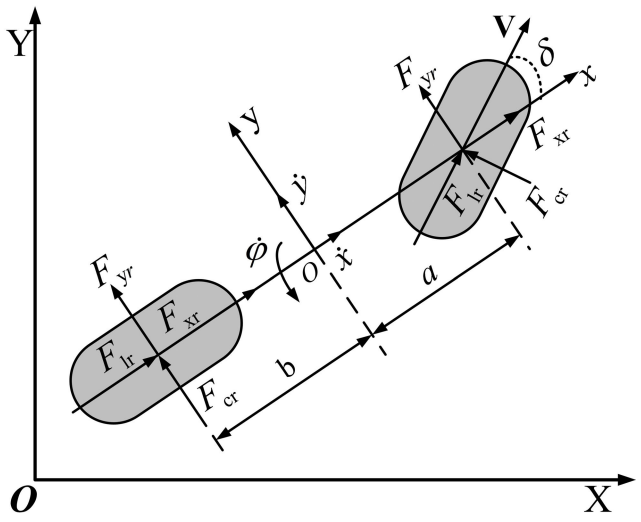

Fig. 2 Three-degree-of-freedom dynamic model

By applying the principles of torque balance, the following differential equation governing the vehicle's motion can be derived:

$$\begin{cases} m\left(\ddot{y}+\dot{x}\dot{\varphi}\right)=2F_{lf}\sin\delta_f+2F_{cf}\cos\delta_f+2F_{cr} \\ m\left(\ddot{y}-\dot{x}\dot{\varphi}\right)=2F_{lf}\sin\delta_f-2F_{cf}\cos\delta_f+2F_{cr} \\ I_z\ddot{\varphi}=2a\left(F_{lf}\sin\delta_f+F_{cf}\cos\delta_f\right)-2bF_{cr} \end{cases} \tag{5}$$

Where m is the mass of the vehicle, F_{yf} and F_{yr} represent the forces along the axis on the wheels. $\dot{\varphi}$ is the vehicle's transverse angular velocity, $\dot{x}$ is the vehicle's transverse velocities, $\dot{y}$ is the vehicle's longitudinal velocities, $\ddot{x}$ is the vehicle's transverse accelerations, $\ddot{y}$ is the vehicle's longitudinal accelerations, I_z is the moment of inertia of the vehicle around the z-axis, , and the F_{xf}, F_{xr} are the forces along the x axis on the wheels. Moreover, y denotes the forces acting on the wheels along the axis, a and b are the lengths from the center of mass to the axles, F_{cf} and F_{cr} are the lateral forces on the front and rear tires, F_{lf} and F_{lr} are the longitudinal forces on the front and rear tires.

The assumptions indicate that the linear slip ratio and tire characteristics to be used as approximations for the longitudinal and lateral forces.

$$F_{cf}=C_{cf}\left(\delta_f-\frac{\dot{y}+a\dot{\varphi}}{\dot{x}}\right) \tag{6}$$

$$F_{cr}=C_{cr}\left(\frac{b\dot{\varphi}-\dot{y}}{\dot{x}}\right) \tag{7}$$

$$F_{lf}=C_{lf}S_f \tag{8}$$

$$F_{lr}=C_{lr}S_r \tag{9}$$

Where C_{lf} and C_{lr} denote the rigidity of the leading and back tires along the longitudinal axis, C_{cf} , C_{cr} denote the stiffness of the front and rear tires, S_f denotes the slip rates of the front tires, S_r is the slip rates of the rear tires.

To simplify the model, trigonometric functions for small angles can be approximated using the following relationships:

$$\sin\theta\approx\theta,\cos\theta\approx 1,\tan\theta\approx\theta \tag{10}$$

By incorporating the simplified equation into the vehicle's differential equation (5), we obtain a nonlinear vehicle dynamics model:

$$\begin{cases} m\ddot{x}=m\dot{y}\dot{\varphi}+2\left[C_{lf}s_f-C_{cf}\left(\delta_f-\frac{\dot{y}+a\dot{\varphi}}{\dot{x}}\right)\delta_f+C_{lr}s_r\right] \\ m\ddot{y}=-m\dot{x}\dot{\varphi}+2\left[C_{cf}\left(\delta_f-\frac{\dot{y}+a\dot{\varphi}}{\dot{x}}\right)\delta_f+C_{cr}\frac{b\dot{\varphi}-\dot{y}}{\dot{x}}\right] \\ I_z\ddot{\varphi}=2\left[aC_{cf}\left(\delta_f-\frac{\dot{y}+a\dot{\varphi}}{\dot{x}}\right)-bC_{cr}\left(\frac{b\dot{\varphi}-\dot{y}}{\dot{x}}\right)\right] \end{cases} \tag{11}$$

III. Path Tracking Lateral Controller Design

A. Design of path tracking controller based on improved pure pursuit algorithm

The PP algorithm reduces the vehicle model to a simplified bicycle model. By applying the kinematic relationship between the target path and vehicle model, the algorithm computes the optimal front wheel angle at each moment, as shown in Fig. 3 below.

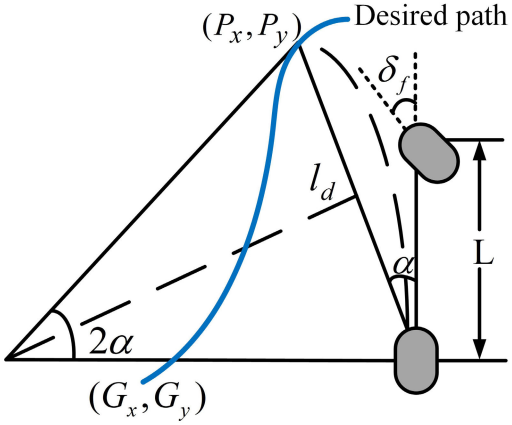

Fig. 3 Pure Pursuit Control Principle

In the Fig. 3, α represents the angle formed between car's longitudinal axis and pre-sighting point, R denotes the turning radius of the car, l_d represents the pre-sighting distance, δ_f represents the frontal wheel's position, (P_x, P_y) denotes the pre-sighting point, (G_x, G_y) represents a target point, L represents the wheelbase.

From the geometric relationship shown in Fig. 3:

$$\frac{l_d}{\sin 2\alpha}=\frac{R}{\sin\left(\frac{\pi}{2}-\alpha\right)} \tag{12}$$

$$R=\frac{l_d}{2\sin\alpha} \tag{13}$$

The following expression is derived from Ackermann's steering theorem:

$$\tan\left(\delta_f\right)=\frac{L}{R} \tag{14}$$

Combining equations (13) and (14) yields:

$$\delta_{f1}(t)=\tan^{-1}\left(2L\sin\alpha(t)/l_d\right) \tag{15}$$

From equation (15), it is evident that the length of the pre-scanning distance is crucial for the effectiveness of path tracking. A short pre-scanning distance can induce oscillations during steering, leading to poor tracking performance and reduced vehicle stability. In contrast, an excessively long pre-scanning distance can degrade tracking accuracy and result in shortcutting during cornering. Therefore, the formula for calculating the optimal pre-scanning distance is given as follows:

$$l_d = AV^2 + BV + C \tag{16}$$

In the formula, *A, B, and C* are constant terms, $a_{\max}$ represent the vehicle's maximum braking and $a_{\max} = 3m/s^2$.

After determining the pre-scan length, the location of the pre-scan point must be identified, as shown in Fig. 4. First, the closest point to the ideal path M_0 is selected as target point. A circle is then constructed, using the target point as its center and the pre-scan length as the radius. This results in two intersection points between the target path and the circle, requiring identification of the correct pre-scan point. By utilizing the car's position and the angle of intersection, leaving the correct pre-scan point M_1.

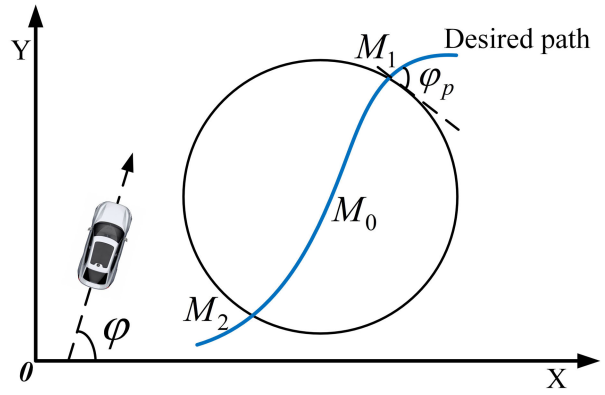

Fig. 4 Schematic diagram of determined preview points on the expected path

Due to the complexity of driving conditions and external disturbances, feed-forward control alone cannot effectively compensate for heading deviation. Therefore, a feedback control system is essential to mitigate the impact of heading errors and achieve the desired control performance. As shown in Fig. 4, φ represents the vehicle's present direction angle, and φ_p denotes the present direction angle at the pre-sight point. As a result, equation (17) can be derived as follows:

$$e_p = \varphi_p - \varphi \tag{17}$$

Most existing methods, such as PID controllers, use fixed coefficients to address heading deviation, which limits their real-time adaptability to dynamic changes in the controlled object. In contrast, the PSO algorithm adjusts PID coefficients in real-time, enhancing the system's flexibility and performance. Equation (18) presents the key speed and position update formulas used in this algorithm:

$$\begin{cases} v_i^{k+1} = \omega v_i^k + c_1 r_1 \left(pbest_i^k - x_i^k \right) + c_2 r_2 \left(gbest_i^k - x_i^k \right) \\ x_i^{k+1} = x_i^k + v_i^{k+1} \end{cases} \tag{18}$$

The c_1, c_2 denotes the learning factor, used to control the extent to which individual particles learn the optimal value each time. r_1, r_2 is an arbitrary number uniformly distributed between the range of [0,1], which increases the randomness of the algorithm searching in a particular area, ω represents the inertia weight, x_i denotes the position and v_i is the velocity of the grain, respectively, *gbest* denotes the position of the best record of the whole population, and *pbest* denotes the position of the best record in the history of an individual particle in the i dimension.

In this paper, the objective function being optimized using particles encoded with a decimal three-dimensional encoding scheme. Fig. 5 below illustrates the underlying principle:

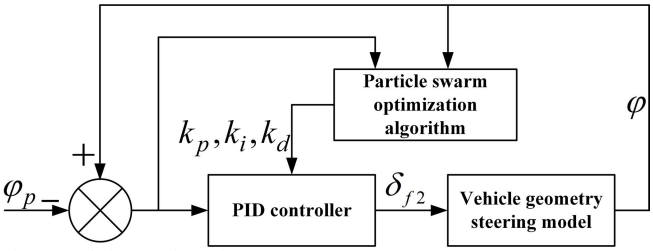

Fig. 5 Real-time tuning of PID parameters

After optimization, the PID control parameters with real-time performance can be obtained using $\left(k_p, k_i, k_d\right)$. The function to be optimized is as follows:

$$obj.f = \sum_{m=0}^{t} \left[\varphi_p(m) - \varphi(m) \right] \tag{19}$$

In the above equation, the objective function represents the moment, where *t* denotes the current time. This allows the PID control parameters, with real-time performance, to be determined using the $\left(k_p, k_i, k_d\right)$. The subsequent equation for the front wheel angle can be derived:

$$\delta_{f2}(t) = k_p e_p(t) + k_i \sum_{m=0}^{t} e_p(m) + k_d \left(e_{p(t)} - e_p(t-1) \right) \tag{20}$$

The following equation illustrates the relationship between the final front wheel angle control quantities:

$$\delta_{final} = k_1 \delta_{f1} + k_2 \delta_{f2} \tag{21}$$

The above equation k_1, k_2 denotes the weight coefficients, which sum to 1.

B. Lateral controller design based on the model predictive control algorithm

The correlation between condition and control factors within the path-tracking system during every certain moment is articulated by equation (22).

$$\dot{\xi}_t = f\left(\xi_x, u_x\right) \tag{22}$$

A Taylor expansion around the point $\left(\xi_x, u_x\right)$, yields the following equation:

$$\dot{\xi} = f\left(\xi_x, u_x\right) + J_f\left(\xi\right)\left(\xi - \xi_x\right) + J_f\left(u\right)\left(u - u_x\right) \tag{23}$$

Where $J_f\left(\xi\right)$ is the Jacobian matrix of f with respect to ξ, and $J_f\left(\xi\right)$ is the Jacobian matrix of f equivalent to u. The equations can be derived as follows:

$$\dot{\tilde{\xi}} = A(t)\tilde{\xi} + B(t)\tilde{u} \tag{24}$$

Where $\tilde{\xi}=\xi-\xi_x, \tilde{u}=u-u_x, A_t=J_f(\xi), B(t)=J_f(u)$

Therefore, a new state equation can be derived. However, since this state equation is continuous, it must be discretized in order to construct a predictive controller. In this study, we apply an approximation method for discretization, as follows:

$$A_{k,t}=I_n+TA(t) \tag{25}$$

$$B_{k,t}=TB(t) \tag{26}$$

Where T is the linear discrete system sampling time (control layer sampling period), I_n is the unit matrix. The above equation (25) and equation (26) can be obtained:

$$\tilde{\xi}(k+1)=A_{k,t}\tilde{\xi}(k)+B_{k,t}\tilde{u}(k) \tag{27}$$

In the system studied in this section, the state variables are defined as $[X,Y,\dot{x},\dot{y},\varphi,\dot{\varphi}]$, and the control inputs are designated as $u=[\delta]$.

From equation (27), it can be inferred that this linearized state-space equation constrains the u_k, but does not limit its increment. Therefore, further transformation of this equation is required, which necessitates the introduction of a new variable χ_k. Thus, equation (28) is obtained:

$$\chi_k=\begin{bmatrix}\tilde{\xi}_k\\ \tilde{u}_{k-1}\end{bmatrix} \tag{28}$$

Equation (27) can then be substituted into (28) to obtain:

$$\chi_{k+1}=A_{k,t}\chi_{(k)}+\tilde{B}_{k,t}\Delta u(k) \tag{29}$$

$$A_{k,t}=\begin{bmatrix}A_{k,t} & B_{k,t}\\ 0_{m\times n} & I_m\end{bmatrix}, \tilde{B}_{k,t}=\begin{bmatrix}B_{k,t}\\ I_m\end{bmatrix}, \Delta u_{(k)}=\tilde{u}(k)-\tilde{u}(k-1)$$

To reduce the computational complexity of the model, equation (29) is simplified by further assumptions:

$$\begin{aligned}A_{k,t}&=A_{t,t}, k=t,t+1,\cdots t+N_p-1\\ B_{k,t}&=B_{t,t}, k=t,t+1,\cdots t+N_p-1\end{aligned} \tag{30}$$

Defining the ρ dimensional output quantity as η gives:

$$\eta(k)=\tilde{C}_{k,t}\chi(k) \tag{31}$$

Assuming that N_p is the prediction time domain and N_c is the control time domain, we can get the equation (32):

$$\Delta u(t+N_c\mid t)=\Delta u(t+N_c+1\mid t)=\Delta u(t+N_p-1\mid t) \tag{32}$$

The system state quantity prediction equation is:

$$\begin{cases}x(t+1\mid t)=\tilde{A}_{t,t}+\tilde{B}_{t,t}\Delta u(t\mid t)\\ x(t+2\mid t)=\tilde{A}_{t,t}^2x(t\mid t)+\tilde{A}_{t,t}\tilde{B}_{t,t}u(t\mid t)+\tilde{B}_{t,t}\Delta u(\mathrm{t+1}\mid t)\\ \vdots\\ x(t+N_c\mid t)=\tilde{A}_{t,t}^{N_c}x(t\mid t)+\tilde{A}_{t,t}^{N_{c-1}}\tilde{B}_{t,t}u(t\mid t)+\cdots+\\ \qquad\tilde{B}_{t,t}\Delta u(\mathrm{t+N_c}-1\mid t)\\ \vdots\\ x(t+N_p\mid t)=\tilde{A}_{t,t}^{N_{p-1}}\tilde{B}_{t,t}u(t\mid t)+\cdots+\\ \qquad\tilde{A}_{t,t}^{N_p-N_c}\tilde{B}_{t,t}\Delta u(t+N_c-1\mid t)\end{cases} \tag{33}$$

Combining equation (31) expresses the system's output prediction equation through a matrix:

$$Y(t)=\Psi_t\xi(t\mid t)+\Theta_t\Delta u(t) \tag{34}$$

Where:

$$Y(t)=\begin{bmatrix}\eta(t+1\mid t)\\ \eta(t+2\mid t)\\ \vdots\\ \eta(t+N_c\mid t)\\ \eta(t+N_p\mid t)\end{bmatrix} \qquad \Psi_t=\begin{bmatrix}\tilde{C}_t\tilde{A}_t\\ \tilde{C}_t\tilde{A}_t^2\\ \cdots\\ \tilde{C}_t\tilde{A}_t^{N_c}\\ \cdots\\ \tilde{C}_t\tilde{A}_t^{N_p}\end{bmatrix}$$

$$\Delta U(t)=\begin{bmatrix}\Delta u(t\mid t)\\ \Delta(t+1\mid t)\\ \cdots\\ \Delta(t+N_c\mid t)\end{bmatrix}$$

$$\Theta_t=\begin{bmatrix}\tilde{C}_{t,t}\tilde{B}_{t,t} & 0 & 0 & 0\\ \tilde{C}_{t,t}\tilde{A}_{t,t}\tilde{B}_{t,t} & \tilde{C}_{t,t}B_{t,t} & 0 & 0\\ \cdots & \cdots & \ddots & \cdots\\ \tilde{C}_{t,t}\tilde{A}_{t,t}^{N_c-1}\tilde{B}_{t,t} & \tilde{C}_{t,t}\tilde{A}_{t,t}^{N_c-2}\tilde{B}_{t,t} & \cdots & \tilde{C}_{t,t}\tilde{B}_{t,t}\\ \tilde{C}_{t,t}\tilde{A}_{t,t}^{N_c}\tilde{B}_{t,t} & \tilde{C}_{t,t}\tilde{A}_{t,t}^{N_{c-1}}\tilde{B}_{t,t} & \cdots & \tilde{C}_{t,t}\tilde{A}_{t,t}\tilde{B}_{t,t}\\ \vdots & \vdots & \ddots & \vdots\\ \tilde{C}_{t,t}\tilde{A}_{t,t}^{N_p-1}\tilde{B}_{t,t} & \tilde{C}_{t,t}\tilde{A}_{t,t}^{N_p-2}\tilde{B}_{t,t} & \cdots & \tilde{C}_{t,t}\tilde{A}_{t,t}^{N_p-N_c-1}\tilde{B}_{t,t}\end{bmatrix}$$

The equation (35) represents the optimization objective function:

$$J(\xi(t),u(t-1),\Delta U(t))=\sum_{i=1}^{N_p}\|\eta(t+i\mid t)-\eta_{ref}(t+i\mid t)\|_Q^2+\sum_{i=1}^{N_c-1}\|\Delta u(t+i\mid t)\|_R^2 \tag{35}$$

The matrices Q,R are the weight and tuning matrices, respectively. The overall expression ensures that the system tracks the target path both quickly and stably. However, during the optimization of the objective function, there may be cases where a solution does not exist. Consequently, an ease element is used to facilitate modifications in the physical values. Consequently, the modified objective function is represented in equation (36).

$$J(\xi(t),u(t-1),\Delta U(t))=\sum_{i=1}^{N_p}\|\eta(t+i\mid t)-\eta_{ref}(t+i|t)-\eta_{ref}(t+i|t)\|_Q^2+\sum_{i=1}^{N_c-1}\|\Delta u(t+i\mid t)\|_R^2+\rho\varepsilon^2 \tag{36}$$

Here ρ is the weight coefficient and ε is the relaxation factor. Matrix calculations are essential for transforming the optimized objective into equation (37).

$$J(\xi(t),u(t-1),\Delta U(t))=[\Delta U(t)^T,\varepsilon]^T H_t[\Delta U(t)^T,\varepsilon]+G_t[\Delta U(t)^T,\varepsilon]+P_t \tag{37}$$

Where: $H_t=\begin{bmatrix}\Theta_t^TQ_e\Theta_t & 0\\ 0 & \rho\end{bmatrix}$,

$$G_t=\begin{bmatrix}2E(t)^TQ_e\Theta_t & 0\end{bmatrix},$$

$$P_t=E(t)^TQ_eE(t),$$

$$E(t)=\Psi_t(t\mid t)-Y_{ref}(t),$$
$$Y_{ref}=[\eta_{ref}(t+1\mid t),\cdots,\eta_{ref}(t+N_p\mid t)]^T.$$

Furthermore, the control inputs and state variables must satisfy specific constraints that are critical for maintaining system stability and ensuring effective control performance. The constraints are as follows:

$$u_{\min}(t+k)\leqslant u(t+k)\leqslant u_{\max}(t+k),k=0,1\cdots,N_c-1 \quad (38)$$

Control of incremental constraints as:

$$\Delta u_{\min}(t+k)\leqslant\Delta u(t+k)\leqslant\Delta u_{\max}(t+k),k=0,1,\cdots,N_c-1 \quad (39)$$

The output constraint is:

$$y_{\min}(t+k)\leqslant y(t+k)\leqslant y_{\max}(t+k),k=0,1,N_c-1 \quad (40)$$

This paper utilizes a linear tire model predicated on the assumption of minimal angles, necessitating the application of suitable limitations on the tire's lateral deflection angle. Consequently, the subsequent limits are imposed on the lateral deflection angle:

$$\begin{cases}\alpha_{\min}-\varepsilon\leqslant\alpha_f\leqslant\alpha_{\max}+\varepsilon\\ \alpha_{\min}-\varepsilon\leqslant\alpha_r\leqslant\alpha_{\max}+\varepsilon\end{cases} \quad (41)$$

The deflection constraint on the center of mass is shown in equation (42).

$$\begin{cases}-12^\circ\leqslant\beta\leqslant12^\circ\ (\text{dry road})\\ -2^\circ\leqslant\beta\leqslant2^\circ\ (\text{icy road})\end{cases} \quad (42)$$

The problem of converting to quadratic programming is shown below:

$$\begin{cases}\min\limits_{\Delta U,\varepsilon}\left[\Delta U(t)^T,\varepsilon\right]^T H_t\left[\Delta U(t)^T,\varepsilon\right]+G_t\left[\Delta U(t)^T,\varepsilon\right]\\ \Delta U_{\min}\leqslant\Delta U(k)\leqslant\Delta U_{\max},k=t,\cdots,t+H_c-1\\ U_{\min}\leqslant u(t-1)+\sum\limits_{i=t}^{k}\Delta U(i)\leqslant U_{\max},k=t,\cdots,t+H_c-1\\ Y_{\min}-\varepsilon\leqslant\Psi_t\xi(t\mid t)+\Theta_t\Delta U\leqslant Y_{\max}+\varepsilon\\ \varepsilon>0\end{cases} \quad (43)$$

The results are derived by solving equation (40) in each operational cycle, thus producing a series control input increases within a control period horizon:

$$\Delta U_t^*=[\Delta u_t^*,\Delta_{t+1}^*,\cdots,\Delta u_{t+N_c-1}^*]^T \quad (44)$$

By modeling the principles of predictive control systems, the following equation is derived:

$$u(t)=u(t-1)+\Delta u_t^* \quad (45)$$

The optimization procedure is utilized to produce a fresh series of control increments. The initial piece of this sequence is chosen and implemented in the system. This cycle continues until the tracking task is fully accomplished.

C. Simulation analysis

Simulation assessments of double-shifted lines within the Carsim/Simulink integrated simulation platform to appraise the control efficacy of the aforementioned two ways. The simulation is carried out at different speeds on a selected pavement, which has a coefficient of friction of 0.85.

The reference model for the driverless vehicle is based on a specific company's vehicle, and Table I below presents the parameter values for this reference model.

TABLE I
MAIN VEHICLE PARAMETERS

Parameters	Value	Unit
Vehicle quality	1350	kg
Center of mass to front axle distance	1000	mm
Center of mass to rear axle distance	1030	mm
Moment of inertia	4126	$kg.m^2$
Front-wheel lateral deflection stiffness	56700	$N.rad^{-1}$

Table II below lists several parameters of the MPC utilized in the simulation validation.

TABLE II
CONTROLLER PARAMETERS

Parameters	Value
Predictive time domain N_p	25
Control time domain N_c	15
The weighting matrix Q	diag [200 100 100]
The weighting matrix R	[5 × 100000]
Relaxing factor ρ	1000
Sampling time T	0.05s

Double-shifted paths are selected for the simulation comparison to assess the work of the two tracking control methods discussed previously.

The formula for the double-shift curve is presented below:

$$Y=\frac{d_{y1}}{2}\left(1+\tanh(z_1)\right)-\frac{d_{y2}}{2}\left(1+\tanh(z_2)\right) \quad (46)$$

Where, $z_1=\frac{2.4}{25}(X-27.19)-1.2,$

$$z_2=\frac{2.4}{21.95}(X-56.46)-1.2,$$
$$d_{y1}=4,d_{y2}=5.75.$$

1) These two control methods are validated by performing path tracking simulations at 10 km/h intervals at speeds ranging from 5-85 km/h. The combined deviation results, derived from equation (47), are analyzed as a comparison index.

$$S_e=k\int_{x_0}^{x_f}|y_1-y_2|dx+(1-k)E_l \quad (47)$$

In the formula, $\int_{x_0}^{x_f}|y_1-y_2|dx$ represents the area bounded by the sideways divergence towards the intended trajectory and the axis x, $y_1=f(x_1)$ is the actual path expression, $y_2=f(x_2)$ is the desired path expression, E_l represents the maximum lateral error during the tracking process, k denotes the weight coefficient, and the value of k is taken to be 0.5, taking into account the full consideration of the tracking control accuracy and the impact of E_l. The findings are presented in Fig. 6 below:

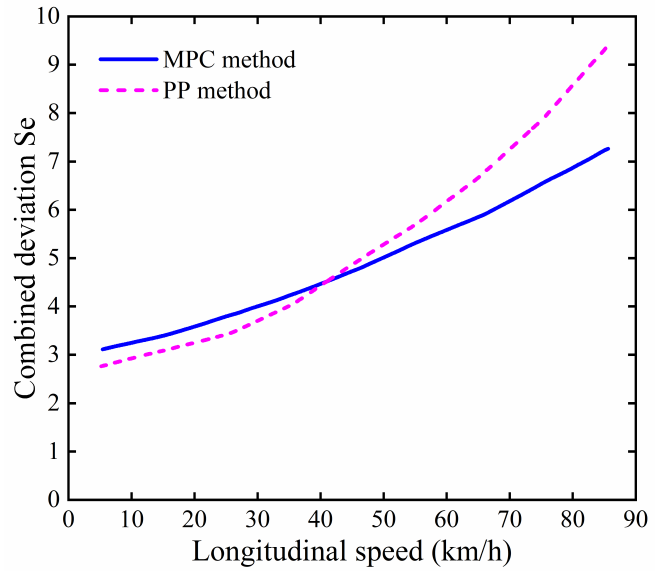

Fig. 6 Comprehensive deviation comparison at different speeds

Fig. 6 represents that path tracking wrong of the PP is inferior than the MPC at velocities below 40 km/h. As the speed of the car increases, the difference becomes more and more obvious, Consequently, 45 km/h is designated as the threshold for differentiating between low and high speeds, as a significant trend alteration transpires at this juncture, emphasizing the distinct performance attributes of the two approaches at disparate speeds.

2) The simulation results are shown in Figs. 7, 8, 9, and 10 for speeds of 30 and 45 km/h, respectively.

As demonstrated in Fig. 7 and Fig. 9, both control methods successfully achieve path tracking, although their tracking accuracy varies with speed. The tracking performance of both methods is sensitive to the changes in vehicle speed, and the effectiveness of each approach becomes more apparent when analyzing the outcomes at varying velocities. In Fig. 8, with a vehicle traveling at 30 km/h, the proportional–proportional control method demonstrates a highest lateral deviation of 0.17 m, but the MPC method approach results in a max lateral deviation of 0.21 m. This indicates that, at this speed, the PP method achieves better tracking accuracy compared to the MPC method. In Fig. 10 illustrates that at 45 km/h, the lateral error for PP method reaches 0.42 m, while the MPC method has a peak lateral error of 0.30 m. At this higher speed, the MPC method exhibits superior tracking performance, with reduced lateral error, indicating its better adaptability to faster driving conditions.

By examining Figs. 6, 7, 8, 9and 10, it is evident that the PP control algorithm performs well at low speeds, demonstrating superior tracking accuracy and robustness under such conditions. However, as the vehicle speed increases, the kinematic model applied in the PP algorithm becomes less effective in accurately capturing the vehicle's dynamics, which leads to a gradual decline in its control performance. In higher-speed scenarios, factors such as vehicle inertia, steering response, and road conditions become more significant, making it more challenging for the PP method to maintain its accuracy. In contrast, the MPC method, which incorporates a more comprehensive kinematic model, maintains higher tracking accuracy. This is due to its ability to integrate kinematic constraints on control volume, control increment, and output, allowing for more precise control in dynamic conditions. As a result, the MPC method demonstrates more consistent and reliable tracking performance under higher-speed driving conditions, where more complex dynamics must be considered.

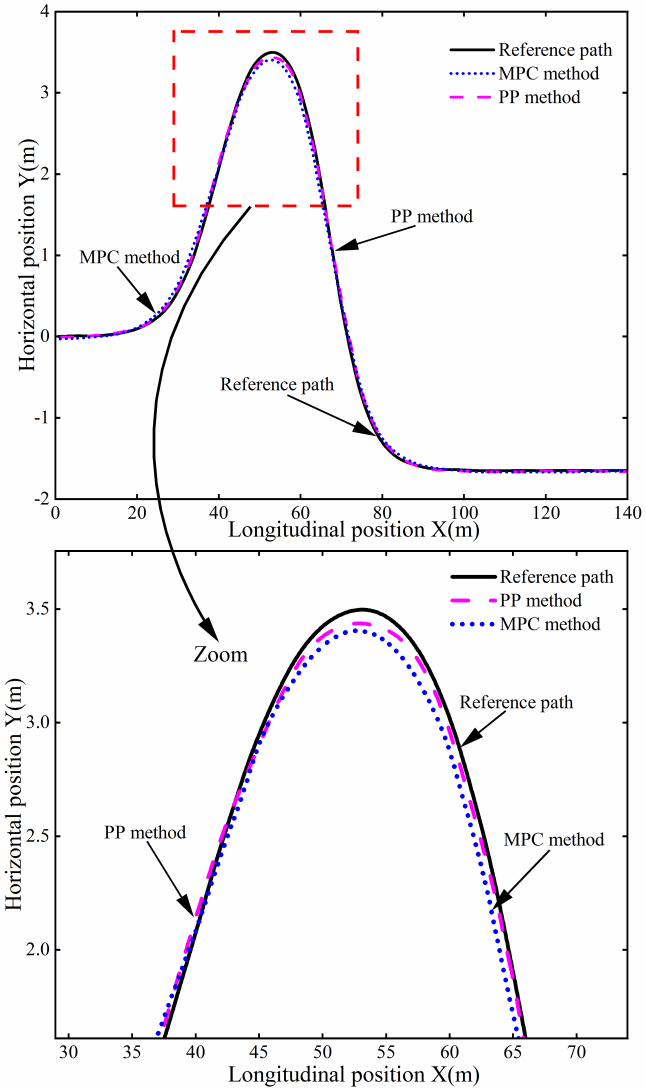

Fig. 7 Path tracking performance at 30 km/h

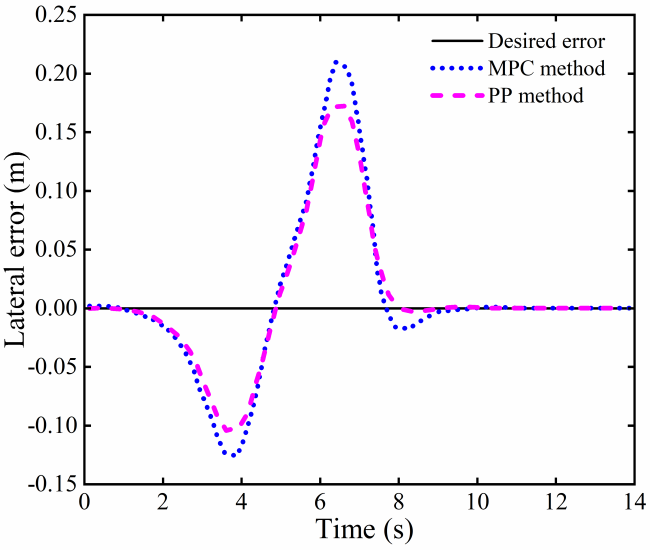

Fig. 8 Comparison of lateral error at 30 km/h

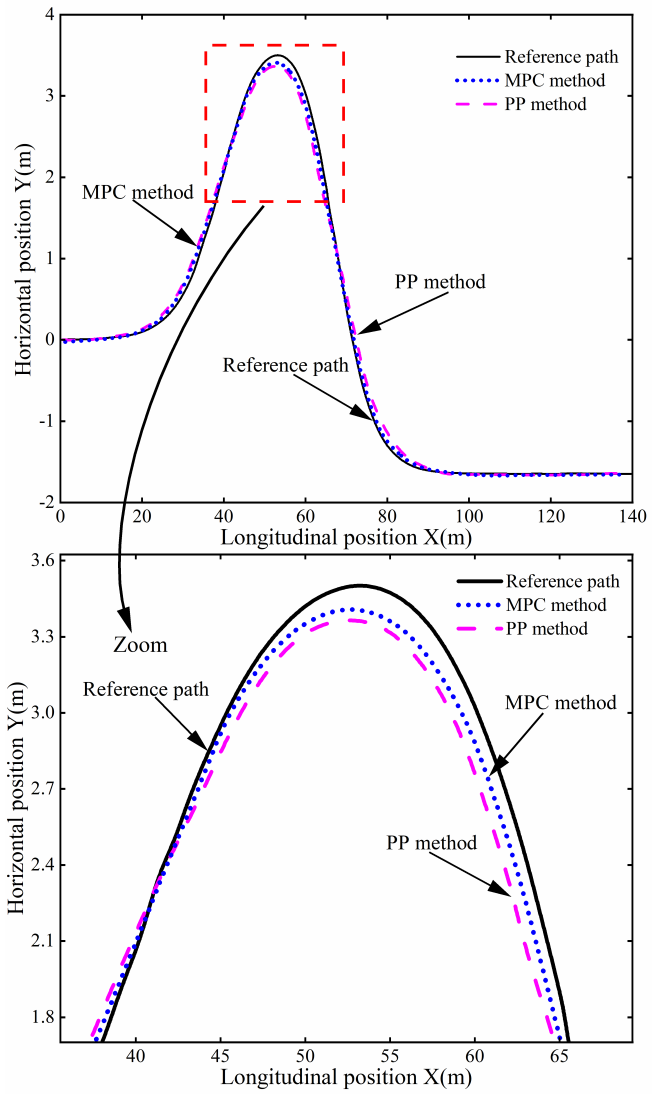

Fig. 9 Path tracking performance at 30 km/h

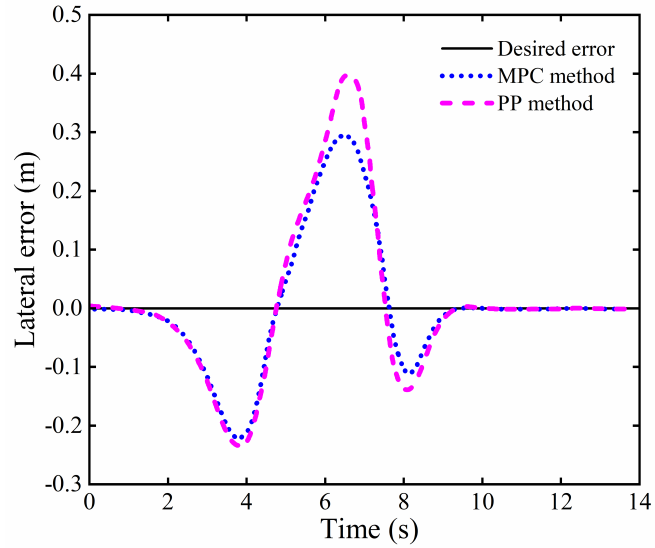

Fig. 10 Comparison of lateral error at 30 km/h

IV. Research on Hybrid Control Method Based on Fuzzy Control

The outcomes of the simulation presented in the preceding chapter highlights the differences in path tracking accuracy between the PP method and the MPC method under varying vehicle speed conditions. This chapter addresses the limitation of relying on a single control algorithm, which may not meet the accuracy requirements for path tracking in driverless vehicles operating across a range of speeds. To overcome this limitation, a hybrid control approach is proposed that combines the strengths of both the pure pursuit and model predictive control algorithms.

A. Hybrid control switching logic design

The vehicle's speed is classified into three distinct intervals: State 1 corresponds to low-speed mode (0–30 km/h), State 2 represents medium-velocity mode (30–45 km/h), and State 3 refers to high-speed mode (above 45 km/h). The switching index is determined by the vehicle's longitudinal velocity. In low- velocity mode (State 1), the controller employs the PP control method, yielding output λ_1. In medium-speed mode (State 2), the controller generates a weighted combination of both control methods, operating them simultaneously. In high-speed mode (State 3), the MPC method is applied, yielding output λ_2. As shown in Fig. 11 below.

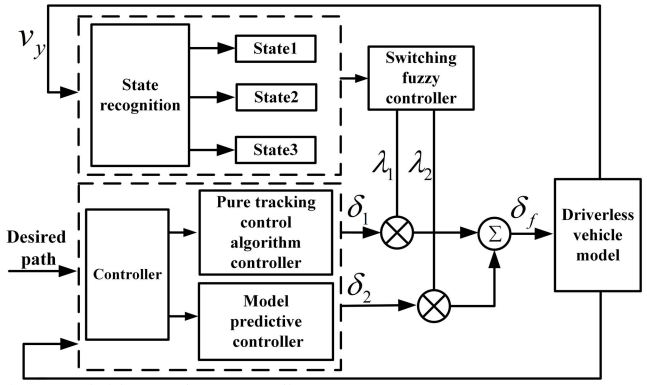

Fig. 11 Hybrid control structure diagram

When the vehicle reaches medium speed, the system transitions into a switching condition, the front wheel steering angle weighting coefficients, originated from both PP method and the MPC method (denoted as λ_2), are combined. A switching fuzzy controller, based on the judgment of longitudinal velocity, integrates the outputs of PP control (δ_1) and the MPC (δ_2) to ascertain the ultimate magnitude of the forward wheel steering angle (δ_f). This relationship is expressed as equation (48):

$$\delta_f = \lambda_1\delta_1 + \lambda_2\delta_2 \tag{48}$$

The state recognition module determines the vehicle's longitudinal speed using speed sensor V_x, allowing it to classify the vehicle into one of three states: low speed, medium speed, or high speed. When the vehicle functions at either elevated or reduced velocity, one of the two weighting coefficients (λ_1, λ_2) is always set to 0. In medium speed mode, both weighting coefficients (λ_1, λ_2) are utilized to combine the front wheel steering angles derived from PP and MPC algorithms, resulting in the final front wheel steering angle control quantity.

B. Hybrid control switching controller design

The controller inputs consist of the error e, which denotes the disparity among the present output and the desired output, together with the rate of alteration of the fault de. The corresponding outputs are the weighting coefficients, denoted as λ_1 and λ_2, respectively.

1) The theory domain and the associated affiliation function.

The fundamental domain of the controller output deviation e is defined as [-50, 50]. The fuzzy domain is set as {-2, -1, 0, 1, 2}, and the associated fuzzy subsets identified as {NB, NS, ZO, PS, PB}. The fundamental domain for the pace of change of the variance de is established as [-30, 30], and its fuzzy domain is set as {-1,0,1}, with the corresponding fuzzy subsets as {N, ZO, P}, and a Gaussian-type affiliation function is applied to all inputs, as showed in Figs. 12 (a) and (b).

Controller's output quantities encompass the weighting coefficient λ_1 and λ_2, which denotes the weighting coefficients for the initial wheel angle of rotation produced by the controller. Therefore, the basic thesis domains for both outputs should be set to [0,1]. The fuzzy thesis domains are specified as {0,1,2,3}, with the corresponding fuzzy subsets defined as {ZO, PS, PM, PB}. The discrete triangular curved subordination functions shown in Fig. 12(c) are used for both output quantities.

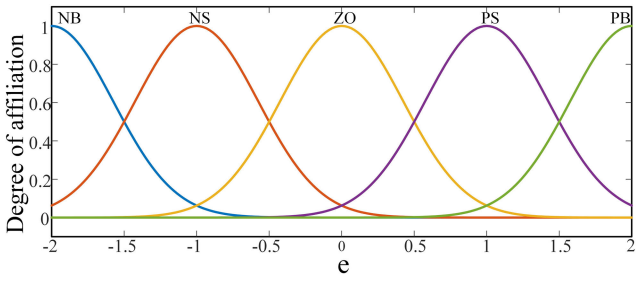

(a) The affiliation function of the deviation e

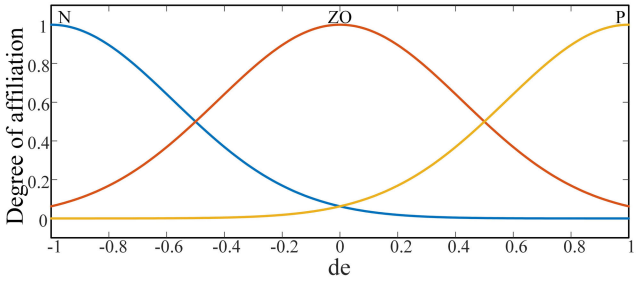

(b) The affiliation function of the rate of change of deviation de

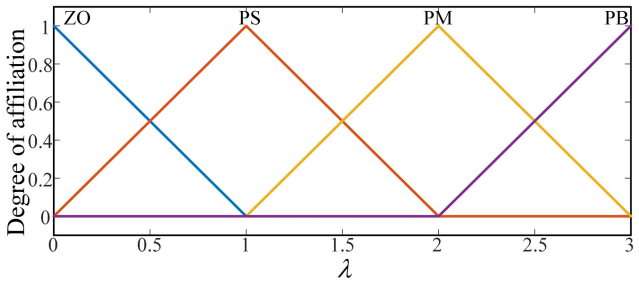

(c) Affiliation function with weighting factor λ

Fig. 12 Membership function

2) Fuzzy rules

The proposed fuzzy control rules are presented in Table III and Table IV below:

TABLE III
WEIGHTING COEFFICIENT λ_1 CONTROL RULES

exports λ_1		control volume deviation				
		NB	NS	ZO	PS	PB
Rate of change of control volume deviation	N	PM	PS	PS	PS	PB
	ZO	PM	PS	ZO	PS	PM
	P	PB	PM	PS	PM	PB

TABLE IV
WEIGHTING COEFFICIENT λ_2 CONTROL RULES

exports λ_2		control volume deviation				
		NB	NS	ZO	PS	PB
Rate of change of control volume deviation	N	PS	PM	PB	PM	PS
	ZO	PS	PM	ZB	PM	PS
	P	PS	PS	PB	PS	PS

Below are a few examples of the representative rules described above:

1) When the deviation of the control quantity is slightly positive and the divergence is changing at an adverse rate, this signifies that the discrepancy between the real production and the desired output is little, and the variance is anticipated to diminish further. In this case, both weighting coefficients should be set to moderate values, including weighting coefficient λ_1.

2) When the two the control deviation and the pace of shift of the deviation are null, it indicates that the target output and the actual output are nearly identical, with no significant trend of change. In this case, the control outputs of both the PP and MPC methods are approximately equal. Therefore, the weighting coefficient should be set to zero under these conditions. Conversely, the weighting coefficient λ_2 should be assigned its maximum value at this point.

As shown in Fig. 13 and Fig. 14, the control surfaces of the weighted coefficients 1 and 2 outputted by the fuzzy controller.

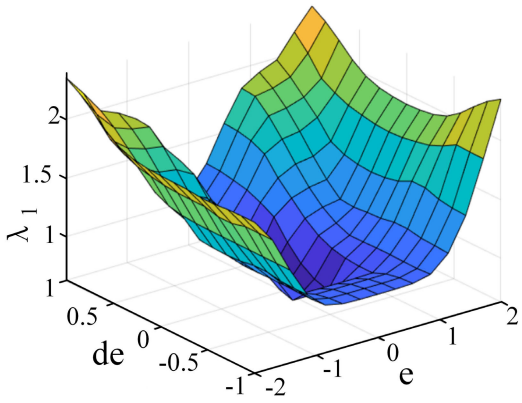

Fig. 13 Output weighting coefficient 1 control surface

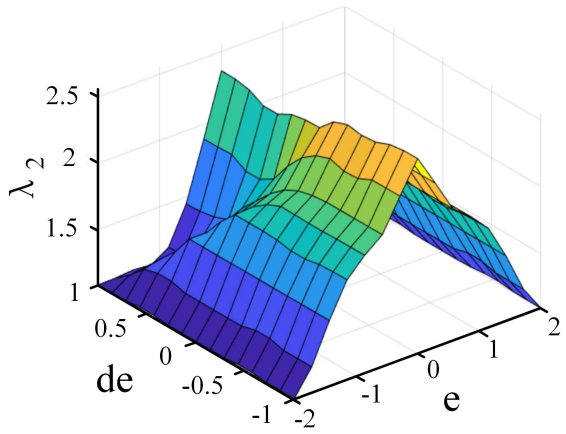

Fig. 14 Output weighting coefficient 2 Control surface

3) Defuzzification

The center of gravity (COG) method offers advantages such as smooth output and high sensitivity, enabling significant variation in fuzzy inference results with even minimal changes in input variables. This characteristic makes the COG method particularly well-suited for applications that require precise control and responsiveness. Consequently, this paper adopts the COG method for defuzzification, extracting the crisp output from the fuzzy inference system. The output is the region beneath the member value curve, bounded by the X-axis and the coordinate axes, which corresponds to the controller's output. This process ensures that the fuzzy system's outputs are effectively transformed into actionable control values, facilitating real-time decision-making within the hybrid control strategy.

V. Simulation

The vehicle speed is set to 40km/h and the road surface adhesion coefficient is 0.85, and the simulation is carried out under the following three conditions, in which the MPC method represents the single control method.

A. Double-shifted line condition

This simulation is conducted under typical conditions, corresponding to a moderately dry road, and set the speed to 40 km/h. The outcomes of the simulation, encompassing the efficacy of the control approaches under these settings, are illustrated in Figs. 15, 16, 17 and Table V below.

According to Fig. 15, both the single and hybrid control methods effectively track the desired path under the specified vehicle speed and operating conditions. Fig. 16 illustrates the lateral error experienced during the trajectory monitoring procedure. The maximum lateral error for the single control method reaches 0.27 m, whereas the hybrid control approach yields a diminished highest lateral error at 0.22 m. This is a significant devaluation in peak error of 18.5%. Additionally, Fig. 17 illustrates a comparison of front wheel angles, indicating that the single control method achieves a maximum front wheel angle of 6.5°, whereas the hybrid control method records a maximum angle of 5.7°. This indicates a 12.3% reduction in the top initial wheel turning angle for the hybrid technique. The simulation findings unequivocally indicate that the hybrid control method improves control accuracy in a double-shift line scenario.

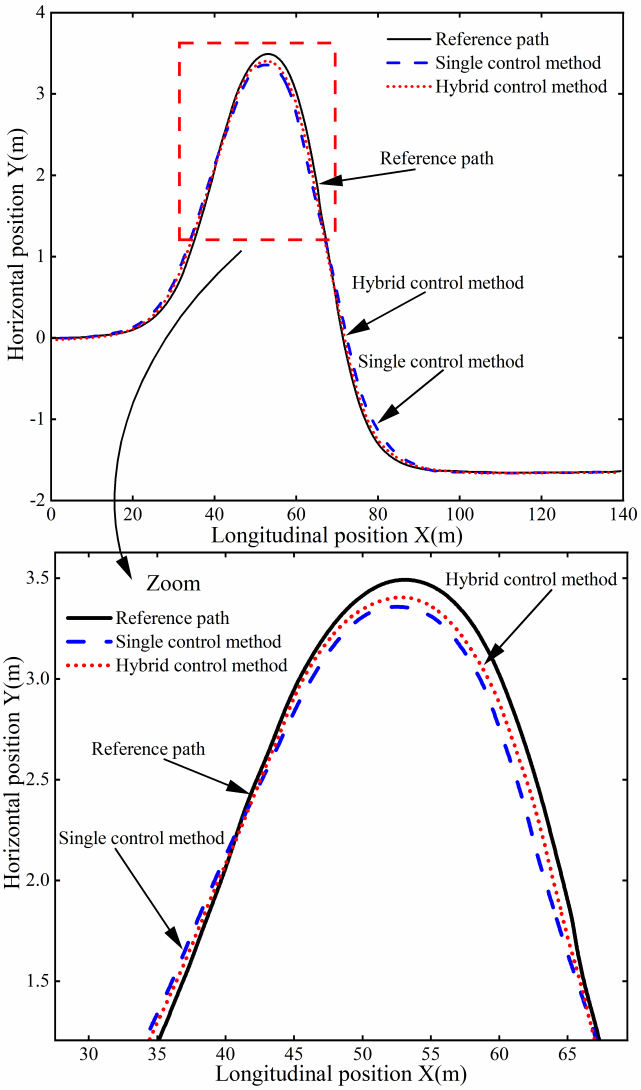

Fig. 15 Path tracking performance under the double-shifted line condition

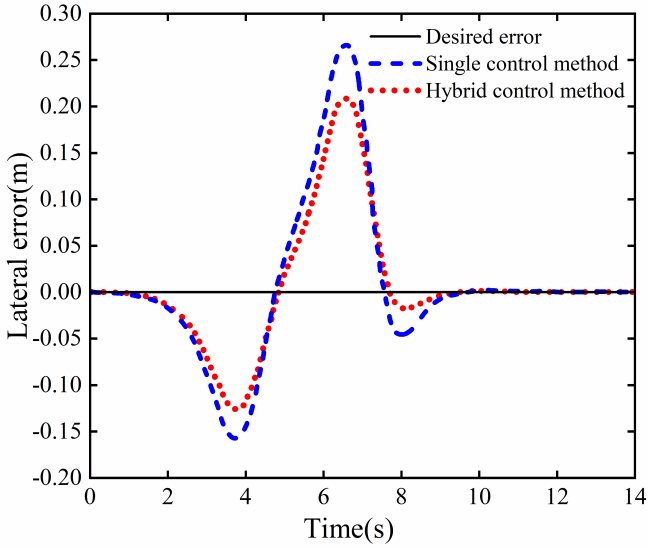

Fig. 16 Comparison of lateral error under the double-shifted line condition

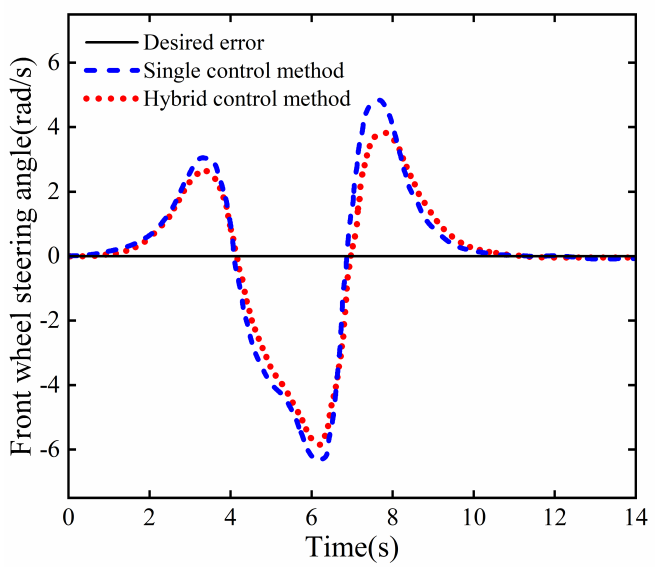

Fig. 17 Comparison of front wheel angle under the double-shifted line condition

TABLE V
COMPARISON OF PATH TRACKING RESULTS UNDER DOUBLE-SHIFT CONDITIONS

Control methods	Single control method	Hybrid control methods	peak-to-peak reduction
$\lvert e\rvert_{max}\ /m$	0.27	0.22	0.05
$\lvert \delta_f\rvert_{\max}\ /deg$	6.5	5.7	0.8

B. *Lane-changing curve condition*

Lane-changing overtaking maneuvers are common conditions for vehicle path tracking control, expression as in equation (49).

$$y=\frac{d}{2\pi}\left[\pi+\frac{2\pi}{l}\left(x-\frac{l}{2}\right)+\sin\left(\frac{2\pi}{l}\left(x-\frac{l}{2}\right)\right)\right] \quad (49)$$

Where d is the car's lateral movement after the lane change, and l is the car's longitudinal motion following the conclusion of the lane shift.

Setting the vehicle speed to 40 km/h, the simulation results are presented in Figs. 18, 19, 20 and Table VI.

Fig. 18 presents the actual driving path alongside the simulation results, comparing the target path with the tracking performance. Both the single and hybrid control methods effectively track the desired trajectory. Fig. 19 illustrates the lateral error during the path tracking process. Maximum lateral error for the single control method reaches 0.28 m, the hybrid control technique attains a maximum inaccuracy of 0.23 m, yielding a notable 17.8% decrease in peak lateral error. This demonstrates the enhanced performance of the hybrid method in minimizing deviation from the desired path.

Furthermore, Fig. 20 compares the front wheel angles during the path tracking process. The single control method exhibits a maximum angle of 5.2°, whereas the hybrid control method records a lower maximum angle of 4.3°. This represents a 17.3% reduction in the peak front wheel angle for the hybrid approach, indicating that it can maintain the desired trajectory with reduced steering input. This attribute substantially enhances the car's overall security during trajectory tracking.

The simulation findings indicate that the hybrid control system additionally accomplishes effective path tracking but also does it with a reduced front wheel angle. This reduction in steering angle is crucial for enhancing the stability of vehicle path tracking.

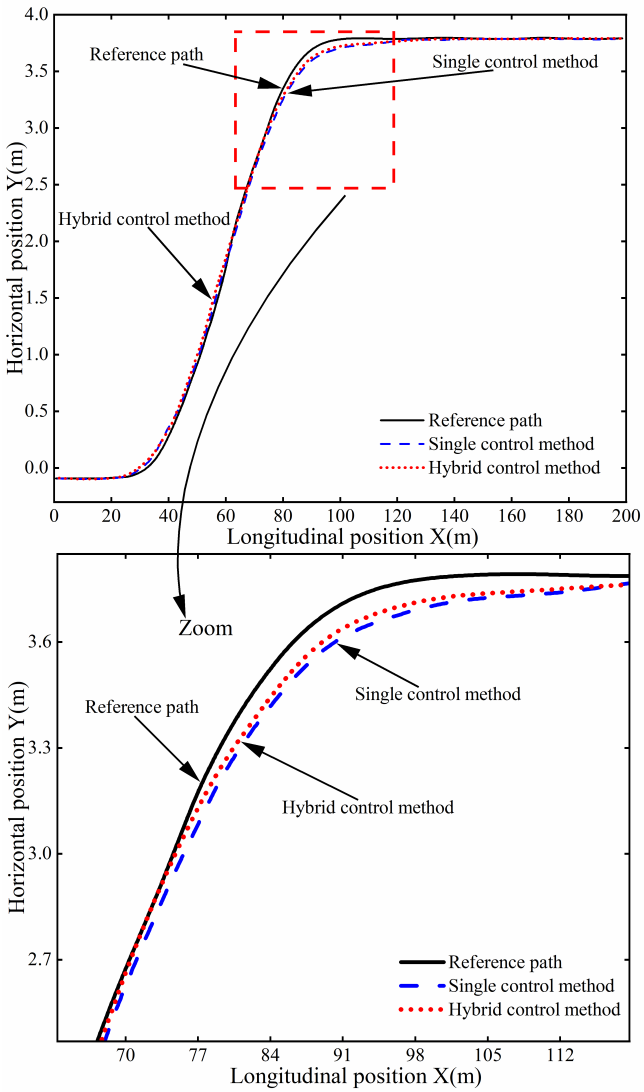

Fig. 18 Path tracking performance under the lane-changing curve condition

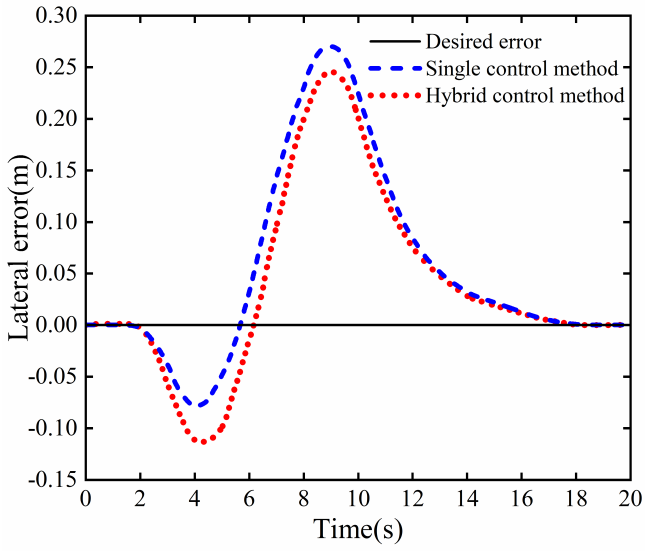

Fig. 19 Comparison of lateral error under the lane-changing curve condition

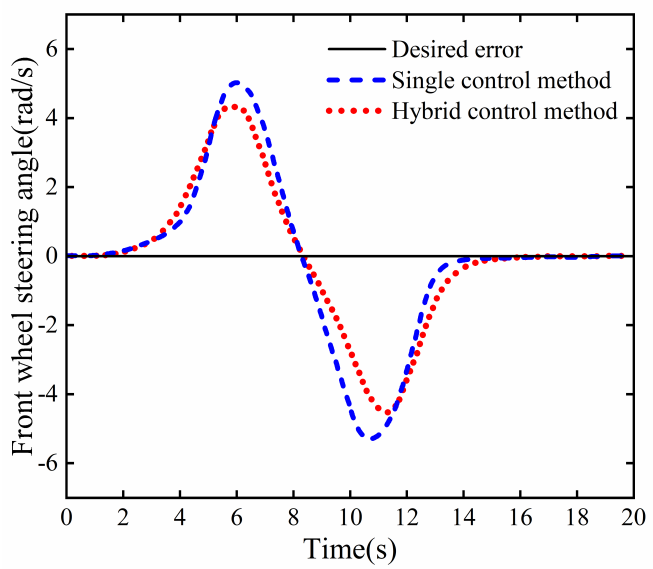

Fig. 20 Comparison of front wheel angle under the lane-changing curve condition

TABLE VI
COMPARISON OF PATH TRACKING RESULTS UNDER LANE-CHANGING CONDITION

Control methods	Single control method	Hybrid control methods	peak-to-peak reduction
$\lvert e \rvert_{max}$ /m	0.28	0.23	0.05
$\lvert \delta_f \rvert_{\max}$ /deg	5.2	4.3	0.9

C. Continuous lane-changing curve condition

Continuous lane-changing is a critical scenario for evaluating the effects of dynamic conditions on path tracking. The car moves at a velocity of 40 km/h, commencing its trajectory at the coordinate origin. The model's outcomes are displayed in Figs. 21, 22, 23, and Table VII below.

Fig. 21 compares the actual driving path with the target route, illustrating that both the single and hybrid control methods are effective in tracking the desired trajectory. Fig. 22 shows the lateral error during the path tracking process. The highest lateral deviation for the singular control approach is 0.38 m. whereas the hybrid control approach attains a reduced maximal transverse error of 0.31 m. This reduction represents an 18.4% improvement in peak lateral error, highlighting the hybrid method's superior performance in maintaining the vehicle alignment with the target path.

Additionally, Fig. 23 illustrates the forward tire angles of the vehicle throughout the route tracking procedure. The single control method exhibits a maximum front wheel angle of 2.5°, whereas the hybrid control method records a lower maximum angle of 2°. This represents a significant 20% reduction in peak front wheel angle for the hybrid approach, indicating that it requires less steering input to maintain the desired trajectory. This efficiency enhances overall vehicle stability and responsiveness.

Though the simulation results reveal continuous fluctuations during dynamic maneuvers, such as lane changes, these variations remain within an acceptable error range. This consistency demonstrates the robustness of both control methods. However, the hybrid control method exhibits higher accuracy and reliability compared to the single control method, making it a more effective choice for complex driving scenarios where precision is crucial.

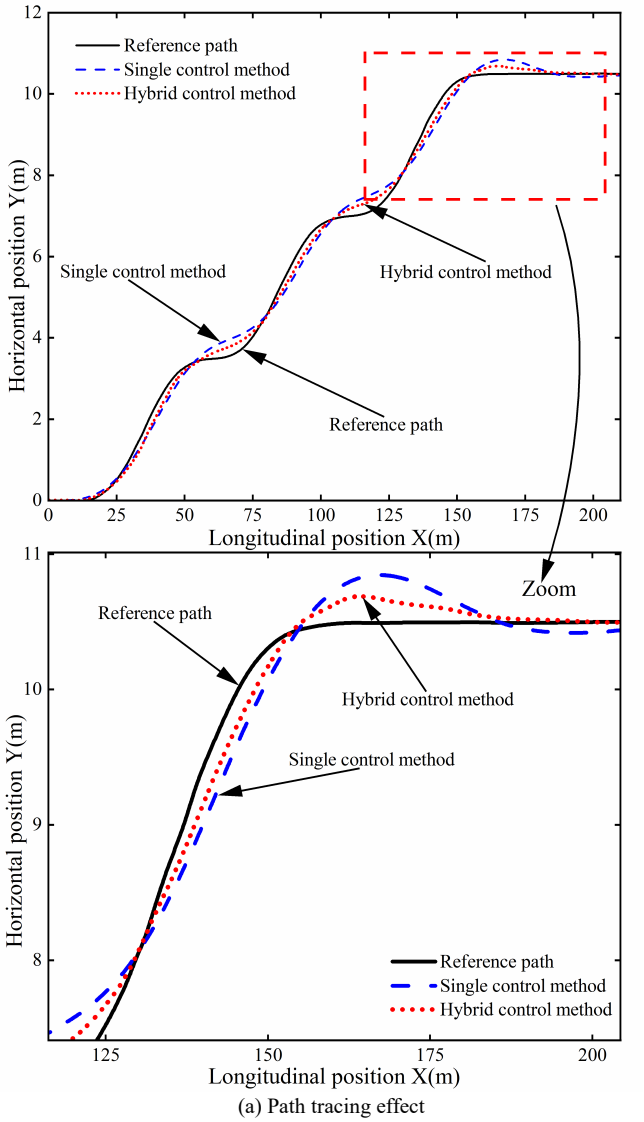

(a) Path tracing effect

Fig. 21 Path tracking performance under the continuous lane-changing curve condition

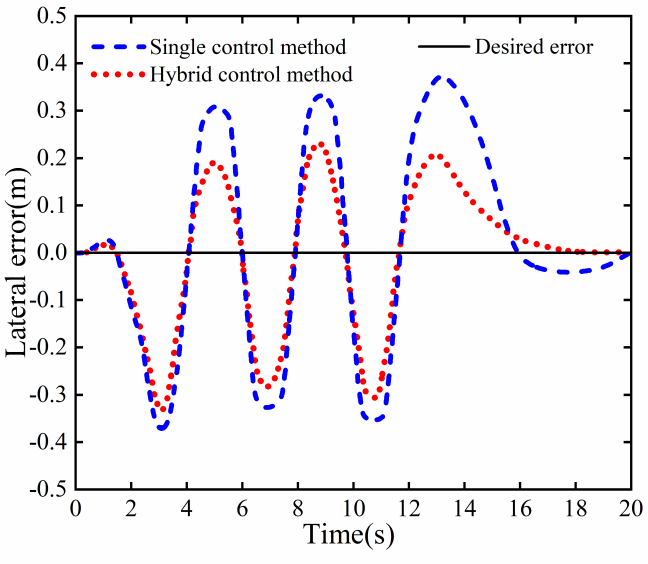

Fig. 22 Comparison of lateral error under the continuous lane-changing curve condition

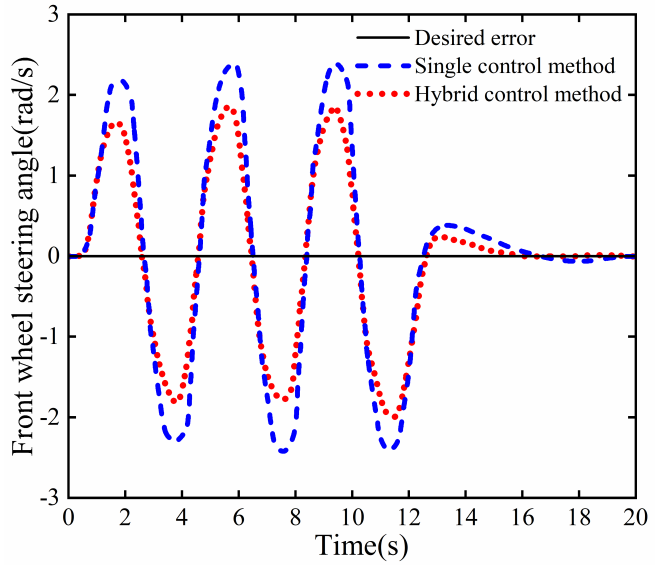

Fig. 23 Comparison of front wheel angle under the continuous lane-changing curve condition

TABLE VII
COMPARISON OF PATH TRACKING RESULTS UNDER CONTINUOUS LANE-CHANGING CURVE CONDITION

Control methods	Single control method	Hybrid control methods	peak-to-peak reduction
$\|e\|_{max}$ /m	0.38	0.31	0.07
$\|\delta_f\|_{\max}$ /deg	2.5	2	0.5

VI. CONCLUSION

This work presents a hybrid control methodology for course tracking in autonomous cars that combines the strengths of both PP and MPC, the conclusions are as follows:

1) The PP method is enhanced by using the vehicle kinematics model. It has been demonstrated that the pure pursuit controller, incorporating pre-scanning, significantly improves tracking performance at lower speeds. Additionally, a path tracking controller founded on the vehicle dynamics framework has been built, incorporating model predictive control. This approach substantially enhances tracking accuracy at higher speeds.

2) A hybrid controller is developed based on fuzzy control theory, combining the advantages of both PP and MPC methods. The controller segments the vehicle longitudinal speed into three distinct intervals, each associated with a specific control method. This strategy ensures that the appropriate control technique is applied within each speed interval, thereby optimizing the system's performance.

3) The hybrid control method's simulation model is executed with the Carsim/Simulink platform, and experimental comparisons are made with a single control method under three distinct working conditions: double-shifted line condition, lane-changing curve condition, and continuous lane-changing curve condition. The experimental findings indicate that the hybrid control strategy significantly improves both path tracking accuracy and driving stability for driverless vehicles across a variety of operating scenarios.

REFERENCES

[1] "Statistical communiqué on the national economic and social development of the people's republic of China for the year 2023," *China Statistics*, vol. 2024, no. 3, pp. 4-21, 2024.

[2] Bari I, Rosen H, Paichadze N, Peden M, and J Monclus Gonzalez, "Global road safety: analysis of global status reports on road safety," *Injury Prevention*, vol. 27, no. Suppl 3, pp. A20-A20, 2021.

[3] Ashley, Grace, Osama A. Osman, Sherif Ishak, and Julius Codjoe, "Investigating effect of driver-, vehicle-, and road-related factors on location-specific crashes with naturalistic driving data," *Transportation Research Record*, vol. 2673, no. 6, pp. 46 – 56, 2019.

[4] Jiancheng C, Zhibin S, Hui Z, and Wanzhong Z, "Path following control of autonomous four-wheel-independent-drive electric vehicles via second-order sliding mode and nonlinear disturbance observer techniques," *IEEE Transactions on Industrial Electronics*, vol. 68, no. 3, pp. 2460-2469, 2021.

[5] Lu X, Xing Y, Guirong Z, and Bo L, "A review of the current development status of motion control for driverless vehicles," *Journal of Mechanical Engineering*, vol. 56, no. 10, pp. 127-143,2020.

[6] Kasper van der El, Daan M. Pool, Marinus René M. van Paassen, and Max Mulder, "Effects of target trajectory bandwidth on manual control behavior in pursuit and preview tracking," *IEEE Transactions on Human-Machine Systems*, vol. 50, no. 1, pp. 68-78, 2020.

[7] Kabzan J, Hewing L, Liniger A, and Melanie N, "Learning-based model predictive control for autonomous racing," *IEEE Robotics and Automation Letters*, vol. 4, no. 4, pp.3363-3370,2019.

[8] Karahan O, and Ataşlar-Ayyıldız B, "Optimal design of fuzzy PID controller with CS algorithm for trajectory tracking control," *Intelligent Computing*, vol. 1, no. 858, pp. 174-188, 2019.

[9] Tao F, Yunpeng W, and Qing L, "Coordinated control of active front steering and active disturbance rejection sliding mode-based DYC for 4WID-EV," *Measurement and Control*, vol. 53, no. 9, pp. 1870-1882,2020.

[10] Yuan Luo, Xianfeng Zhang, and Jinke Wu, "An improved hybrid particle swarm optimization path planning algorithm based on particle reactivation," *IAENG International Journal of Computer Science*, vol. 51, no. 10, pp. 1534-1545, 2024.

[11] P. Wang, S. Gao, L. Li, S. Cheng, and L. Zhao, "Automatic steering control strategy for unmanned vehicles based on robust backstepping sliding mode control theory," *IEEE Access*, vol. 7, pp. 64984-64992, 2019.

[12] Nahlia Rakhmawati, Agus Widodo, Noor Hidayat, and Abdul RoufAlghofari, "Optimal path with interval value of intuitionistic fuzzy number in multigraph," *IAENG International Journal of Computer Science*, vol. 51, no. 1, pp39-44, 2024.

[13] Zhiqiang Z, Mengjia Y, Haoyu W, and Li W, "A lateral control strategy for unmanned ground vehicles with model predictive control and active disturbance rejection control," *Transactions of the Institute of Measurement and Control*, vol. 43, no. 15, pp. 3473-3482, 2021.

[14] Z. Ma, O. Postolache, and Y. Yang, "Obstacle avoidance for unmanned vehicle based on a 2D LIDAR," *International Conference on Sensing and Instrumentation in IoT Era*, pp. 1-6, doi: 10.1109/ISSI47111, 2019.

[15] Yin-Yin Bao, Yu Liu, Jie-Sheng Wang, and Jia-Xu Liu, "Genetic algorithm based on grid maps for solving robot path planning problem," *Engineering Letters*, vol. 31, no. 4, pp. 1635-1648, 2023.

[16] Nur Uddin, Hendra G. Harno, and Wahyu Caesarendra, "Vector-based modeling and trajectory tracking control of autonomous two-wheeled robot," *IAENG International Journal of computer Science*, vol. 48, no. 4, pp. 1049-1055, 2021.

[17] Su S, and Chen G, "Lateral robust iterative learning control for unmanned driving robot vehicle," *Proceedings of the Institution of Mechanical Engineers, Part I: Journal of Systems and Control Engineering*, vol. 234, no. 7, pp. 792-808, 2020.

[18] Hong Chen, "Path planning of mobile robot using hybrid algorithm based on GA-IACO," *Engineering Letters,* vol. 30, no. 2, pp. 582-589, 2022.

[19] Han G, Fu W, Wang W, and Wu Z, "The lateral tracking control for the intelligent vehicle based on adaptive PID neural network," *Sensors*, vol. 17, no. 6, pp. 1244, 2017.

[20] Hu C, Wang R, and Yan F, "Integral sliding mode-based composite nonlinear feedback control for path following of four-wheel

independently actuated autonomous vehicles," *IEEE transactions on transportation electrification*, vol. 2, no. 2, pp. 221-230, 2016.

[21] Sanghyun Hong, and J. Karl Hedrick, "Roll prediction-based optimal control for safe path following," *Proceedings of the American Control Conference*, vol. 2015, pp. 1-6, doi:10.1109/ACC.2015.7171835, 2015.

[22] Kayacan, Erkan, Ramon, Herman, Saeys, and Wouter, "Robust trajectory tracking error model-based predictive control for unmanned ground vehicles," *IEEE/ASME transactions on mechatronics: A joint publication of the IEEE Industrial Electronics Society and the ASME Dynamic Systems and Control Division*, vol. 21, no. 2, pp. 806-814,2016.

[23] Jialing Y, and Zhen G. "Path-tracking control strategy of unmanned vehicle based on DDPG algorithm," *Sensors*, vol. 22, no. 20, pp. 7881-7881, 2022.

[24] Wei W, Huiyan C, Jianhao M, Kai L, and Jianwei G, "Path tracking for intelligent vehicles based on frenet coordinates and delayed control," *Acta Armamentarii*, vol. 40, no. 11, pp. 2336-2351, 2019.

[25] Yong Z, Yu X, Haifei C, Linxion H, and Fengkui Z, "Research on lateral control of intelligent vehicle path tracking," *Journal of Chongqing University of Technology (Natural Science)*, vol. 35, no. 7, pp. 53-61, 2021.

[26] Liang C, Zhaobo Q, Weiwei K, and Xin C, "Lateral control using LQR for intelligent vehicles based on the optimal front-tire lateral force," *Journal of Tsinghua University (Science and Technology)*, vol. 61, no. 9, pp. 906-912, 2021.

[27] Shouwu Z, Qing L, Heng W, and Meng L, "Path following control for autonomous vehicles with mismatched uncertainties," *Control and Decision*, vol. 37, no. 1, pp. 160-166, 2020.

[28] Yifan L, Guanglin S, Yaofeng C, and Lun S, "Fuzzy path following control method based on pure pursuit model," *Machine Design & Research*, vol. 38, no. 3, pp. 136-140+157,2022.

[29] Feng W, Huabing Z, Dongcai Y, and Song G, "Lateral control of intelligent vehicle based on active disturbance reduction technology," *Agricultural Equipment & Vehicle Engineering*, vol. 59, no. 2, pp. 48-53, 2021.

[30] Wei T, Jingsheng L, Hui Z, and Hongqian Q, "Intelligent vehicle path tracking control under parametric uncertainties and external disturbances," *Journal of Zhejiang University (Engineering Science)*, vol. 57, no. 4, pp. 702-711, 2023.